Journal of Nanoparticle Research **5:** 17–30, 2003.

Fabrication of nanomaterials using porous alumina templates

Shoso Shingubara
Graduate School of Advanced Sciences of Matters, Hiroshima University, Kagamiyama 1-3-1, Higashi-Hiroshima 739-8530 Japan (Fax: +81-824-24-7645; E-mail: shingu@hiroshima-u.ac.jp)

Received 6 January 2003; accepted in revised form 29 March 2003

Key words: porous alumina, anodic oxidation, quantum dot, nanorod, photoluminescence, magnetic storage

Abstract

Nanofabrication by self-organization methods has attracted much attention owing to the fact that it enables mass production without the use of expensive lithographical tools, such as an electron beam exposure system. Porous alumina can be fabricated electrochemically through anodic oxidation of aluminum by means of such a self-organization method, yielding highly ordered arrays of nanoholes several hundreds down to several tens of nanometers in size. This paper is an overview of recent research on porous alumina science and technology, nanohole array self-organization conditions and mechanisms, various methods of nanostructure formation using porous alumina templates, optical and magnetic nanofabrication, perspectives on electronic nano device fabrication and chemical/biological sensors and membranes.

Introduction

Porous alumina films formed by anodic oxidation of aluminum have been intensively studied for use as molds to form nanostructured materials. While the technology of porous alumina and its usage as an anodic oxide coating in tools has a long history, basic research on self-organization of nanostructures via porous alumina templates began much more recently, namely in the mid-1990s. There is a great demand for the use of highly ordered nanohole arrays, which can be produced on a scale of several tens of nanometers through self-organization, in a diversity of applications, such as high density storage media, functional nanomaterials exhibiting quantum size effect, highly sensitive chemical sensors, nano electronic devices and functional bio-chemical membranes. This paper reviews recent research activity on nanofabrication by porous alumina templates; it focuses on self-organization conditions and mechanisms, nanostructure formation, optical and magnetic nanomaterials fabrication, electronic nano devices and chemical and biological sensors.

Nanohole array formation and self-organization

Anodic oxide coating for aluminum and aluminum alloys containing various acidic electrolytes has been explored since the early 1900s, and widely used as tableware, kettle, car body and other commodities. In the early days of porous alumina research, Keller et al. (1953) reported details on cell structure and anodic voltage dependence of the cell size. They defined a cell as the unit area containing a single nanohole. Anodically oxidized alumina film consists of nanoholes that grow normal to the surface. Later, several authors discussed the mechanism of nanohole formation by electrical field assisted dissolution (Hoar & Mott, 1959; O'Sullivan & Wood, 1970; Thompson et al., 1978). Thompson et al. discussed the effect of two processes: (i) growth of aluminum oxide at the interface between aluminum and alumina due to transport of Al^{3+}, OH^- and O^{2-} ions within the alumina film and (ii) the dissolution and deposition of aluminum oxide at the interface between the alumina film and solution.

An explosion of porous alumina research was ignited once the capability of producing a nanohole array with excellent regularity was established. Masuda and Fukuda (1995) reported that a highly ordered nanohole array could be obtained by two-step anodization of high purity aluminum using a 0.3 M oxalic acid solution under a constant voltage of 40 V at 0°C. The first anodization is carried out for 160 h. Although cell arrangement at the surface is not so regular, nanohole regularity improves with increasing film thickness. Excellent regularity can be achieved at the hole bottom after a long anodization period. Then the first anodic alumina film is selectively wet etched away by the so-called P-C etch established by Schwartz and Platter (1975), in which a mixture of 35 ml/l 85% H_3PO_4 and 20 g/l CrO_3 at 80°C is used. The post-etched aluminum surface has a periodic surface roughness, as evidenced by a highly regular array of nanohole bottoms. Consequently, the nanohole array formed by the second anodic oxidation exhibits excellent regularity as a result of the initial surface.

Figure 1 shows a typical nanohole array formed by the two-step anodization. A plan view SEM micrograph (Figure 1a) shows a trigonal lattice of nanoholes having an average diameter of 36 nm. The nanoholes are slightly enlarged by wet chemical etching with diluted phosphoric acid; the distance between holes is 90 nm. A cross-sectional view of alumina nanoholes formed by the second, 30 s long anodization is shown in Figure 1b. The hole depth is 220 nm; the hole bottom is closed by a so-called barrier film 30 nm in thickness. Neighboring nanoholes are separated by a 50 nm thick alumina sidewall.

The size and geometrical arrangement of the well-ordered nanohole array is constrained by the self-organization condition that is determined by the acid species. Shingubara et al. quantified the regularity of the nanohole array, in the case of oxalic acid electrolyte, as a function of anodic voltage and acid concentration (Shingubara et al., 1997). The regularity of the nanohole array is the highest around 40 V; it improves with increasing first anodization time and acid concentration. The average cell and hole diameters as a function of anodic voltage are shown in Figure 2. The relationship between cell diameter and voltage is almost linear, however, the cell size drops rapidly below 20 V. Self-organization conditions in the case of sulfuric acid (Masuda et al., 1997a) and phosphoric acid (Masuda et al., 1998) were investigated. The anodic voltage that gives a well-ordered nanohole array is found to be dependent on the acid species.

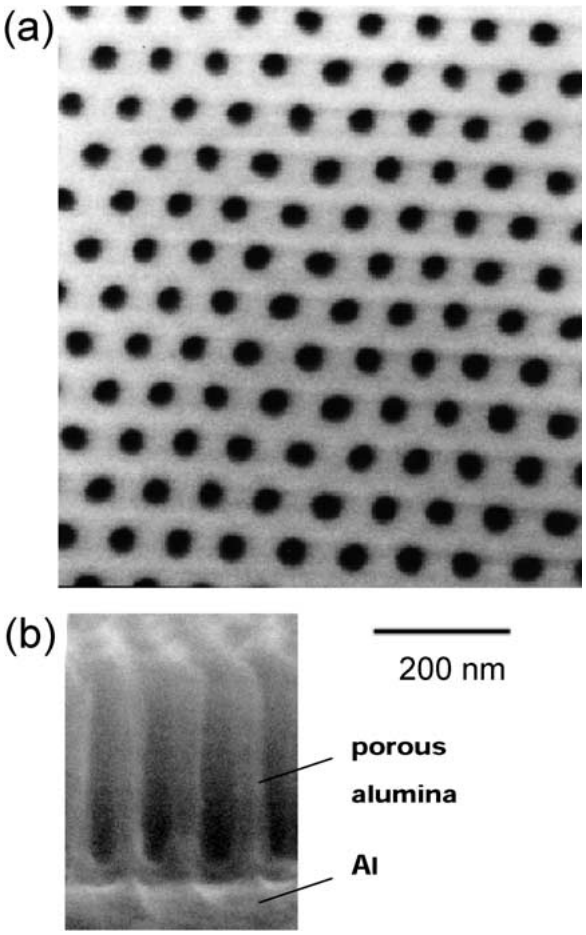

Figure 1. SEM micrographs of alumina nanohole array formed by two step anodic oxidation of 40 V using 0.15 M oxalic acid. (a) plan-view, (b) cross-sectional view (Shingubara et al., 1997).

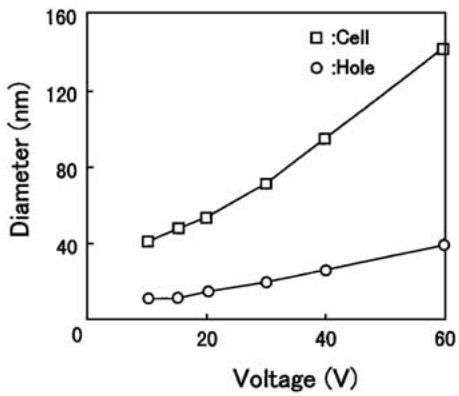

Figure 2. Voltage dependence of nanohole diameter and cell diameter, formed by oxalic anodic oxidation (Shingubara et al., 1997).

Table 1. Nanohole diameter and cell diameter obtained by typical self-organization conditions using different acid species

Acid/voltage	Hole diameter (nm)	Cell diameter (nm)
H_2SO_4/25–27 V	>13	50–60
$(COOH)_2$/40 V	>25	90
H_3PO_4/195 V	>200	500

Typical dimensions of the nanohole array under self-organization conditions are summarized in Table 1. The cell diameter under self-organization conditions are 500, 90 and 50–60 nm for phosphoric acid (anodization voltage $V_a = 195$ V), oxalic acid ($V_a = 40$ V) and sulfuric acid ($V_a = 25$–27 V), respectively. Hole diameters immediately after anodic oxidation are listed in the table; additional diluted phosphorous acid etching can increase these values, i.e., widen the holes. Cell size differs slightly for different acids at a given anodic voltage. For instance, the cell size formed by sulfuric acid is slightly smaller than that formed by oxalic acid when anodic voltage is between 30 and 40 V.

The mechanisms for nanohole self-organization have not yet been satisfactorily identified. Jessensky et al. (1998a,b) discussed the morphology and formation conditions of ordered hexagonal pore arrays for both oxalic and sulfuric acid. They suggested that the voltage dependence of the volume expansion of the aluminum during oxidation and the current efficiency for oxide formation are responsible for the voltage dependence of nanohole self-organization. Nielsch et al. (2002a) proposed that self-ordering requires a porosity of 10%, independent of the specific anodization conditions. They propose that self-ordering of porous alumina is possible with any interpore distance if the applied voltage and the pH value of the electrolyte match the 10% porosity rule. The effect of the stress at the aluminum/porous alumina interface would be an essential part of these volume expansion arguments. We need to further clarify the origin of the nearest neighbor interaction between adjacent nanoholes, since it would produce a close-packed hexagonal lattice in two dimensions.

A new approach to controlling nanohole arrangement by pretexturing the initial aluminum surface was proposed by Masuda et al. (Masuda et al., 1997b; Asoh et al., 2001). They prepared periodic concave regions on the aluminum surface by pressing it using a SiC mold with an array of periodic convex surfaces. Figure 3 schematizes the pretexturing process. The SiC mold was fabricated by conventional lithography

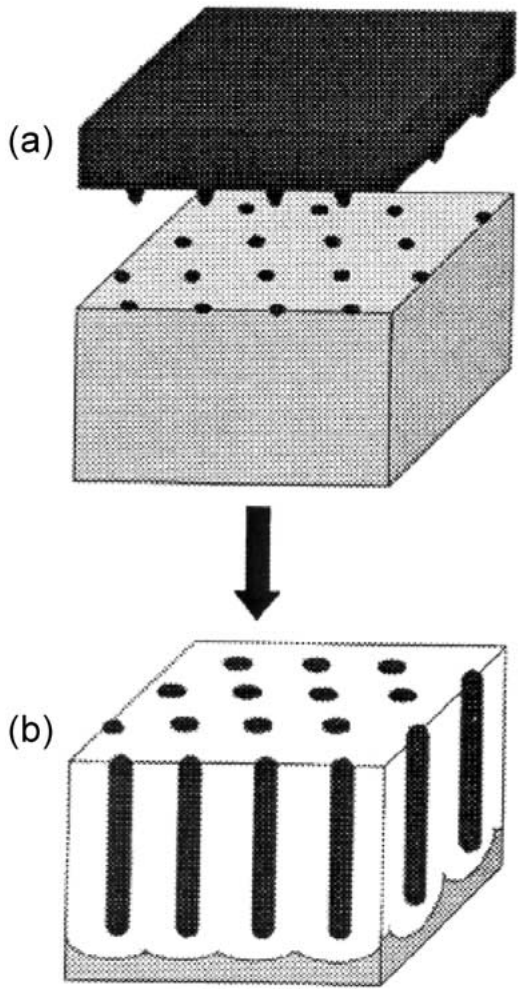

Figure 3. A method to imprint periodic concaves on Al by SiC mold to control nanohole initial position (Asoh et al., 2001).

and dry etching. A long-range-ordered channel array with dimensions on the order of millimeters could be obtained by this method. This method is very effective for fabricating a photonic band crystal that will be mentioned later. The density and hence the fineness of the nanohole array is limited by the electron beam lithography and dry etching of the SiC mold. Even through state-of-the-art electron beam lithography technology, a cell size finer than 50 nm would be too difficult to fabricate in large area. Alternative pretexturing technique using atomic force microscopy (AFM) nano-indentation was proposed (Shingubara et al., 2002a; 2003). A schema of AFM nano-indentation is shown in Figure 4. By using a diamond-tipped AFM, periodic concave regions can be formed with the desired

pitch and geometrical arrangement. Shingubara et al. tried to form a tetragonal array of nanoholes using an aluminum thin film sputtered on a Si substrate, since a tetragonal array tends to rearrange into a trigonal array as the holes deepen. An indenting strength of around 4×10^{-5} N was sufficient to control the initiation of nanohole formation by nano-indentation. The effect of indentation interval on the regularity of nanoholes at a fixed anodic voltage of 40 V is shown in Figure 5. At a 55 nm interval (Figure 5a), nanoholes were connected to each other, and at a 110 nm interval (Figure 5d), additional holes formed at random between the holes whose positions were controlled by indentation. Ordered arrays of nanoholes were formed at 65 and 80 nm intervals. Thus, controllability of nanoholes depends on both anodic voltage and indentation interval.

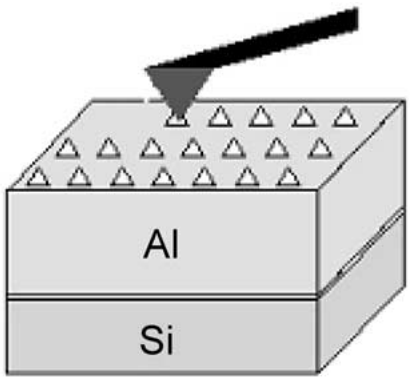

Figure 4. AFM nanoindentation.

Nanofabrication using a porous alumina template

Self-organized porous alumina nanohole arrays have been used to fabricate a variety of nanomaterials. These methods are categorized as follows: etching semiconductor substrate using a porous alumina film as a mask, pattern transfer using porous alumina as a template, deposition of functional materials in the form of porous alumina nanohole arrays by electroplating and sol–gel, and deposition of functional materials by chemical vapor deposition (CVD).

Porous alumina as an etching mask

Pattern transfer of nanoholes to a semiconductor substrate is promising for applications such as photonic band materials, field emitter arrays and quantum dot arrays. In the beginning, a thin porous alumina film was used as a dry etching mask, by placing it in contact with the substrate (Nakao et al., 1999; Liang et al., 2002; Chen et al., 2001). The porous alumina film was delaminated from the aluminum plate by a negative voltage pulse or dissolution of aluminum by dipping in $HgCl_2$ solution. After removal of the nanohole bottom barrier layer by Ar plasma etching or ion beam etching, a porous alumina film is placed on the substrate. Highly directional ion beam etching is necessary for substrate etching since the alumina nanohole aspect ratio (the ratio of depth to diameter) is very high. GaAs and InP substrates by reactive ion beam etching (RIBE) (Nakao et al., 1999; Liang et al., 2002), and an InGaN/GaN

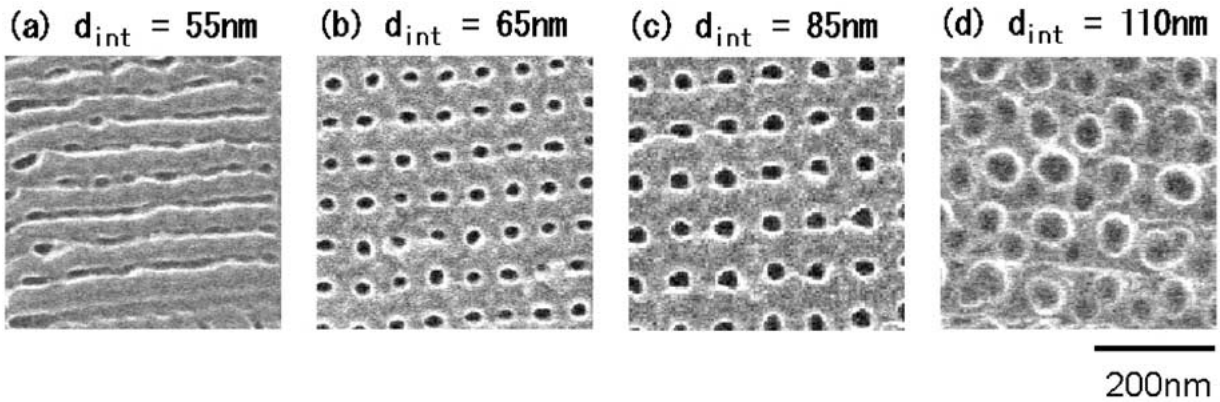

Figure 5. Plan-view SEM micrographs of porous alumina film surfaces that were formed by AFM nano-indentation followed by anodic oxidation at 40 V using 0.15 M oxalic acid for 5 min. Indentation force was 4.16×10^{-5} N. Indentation interval d_{int} was varied from 55 to 110 nm. (Shingubara et al., 2002).

multiple quantum well (MQW) (Chen et al., 2001) were assessed. The alumina mask showed high tolerance to RIBE using a Br_2/N_2 mixed gas system. In this method, maintaining the gap between the porous alumina and the substrate at a minimum is essential for achieving ultrahigh uniformity. Recently, an alternative method, namely using a porous alumina film deposited directly on the semiconductor substrate, was proposed (Shingubara et al., 2001). A thin porous alumina film with an aspect ratio below 5 was formed on a Si/SiO_2 substrate by the use of sputtered aluminum. Reactive ion etching using chlorine with a high self-bias of RF plasma proved effective for pattern transfer to Si. There was a significant reduction in hole size due to redeposition of nonvolatile materials on the sidewall of nanoholes. For instance, the initial porous alumina hole size of 45 nm was reduced to 13 nm Si holes when a higher aspect ratio of porous alumina nanoholes mask was used. The problem with this method is the non-uniformity of the porous alumina mask thickness, which would require a specially designed anodic oxidation electrode to improve.

Pattern transfer by replica of porous alumina film

Pattern transfer of alumina nanohole arrays to metallic hole arrays using a replica was proposed (Masuda & Fukuda, 1995). After detachment of the porous alumina film by wet dissolution of the aluminum substrate using HgCl, the bottom barrier layer was removed by ion beam etching. Then, the negative of the nanohole array pattern was transferred to PMMA by coating it on the porous alumina film. Finally, the porous aluminum film was chemically wet-etched, leaving behind only the resist pattern. The PMMA pattern can be used to form a replica by deposition of metals via sputtering, evaporation, etc.

Electroplating or sol–gel synthesis on porous alumina

Numerous studies have been conducted on filling of conductive materials in porous alumina nanoholes by electroplating. Possible applications include coloring of the aluminum plate itself (Asada, 1969; Gphausen & Schoener, 1984) and magnetic recording media for a high-density magnetic disk (Kawai & Ishiguro, 1975; 1976). Prior to electroplating, the bottom barrier layer should be thinned to less than about 10 nm. Wet chemical etching of the anodic alumina film using a diluted phosphorous acid solution (pore widening treatment), or step-wise lowering of the anodic voltage down to 10 V were employed. Alternating current (AC) or pulsed-current electroplating was used since the impedance of the barrier layer at the nanohole bottom is too large to afford for direct current (DC) electroplating. Research activity on the electroplating of magnetic materials in porous alumina has intensified remarkably in recent years; details will be presented later. As for other metals, nanowire array formation of gold (Shingubara et al., 1997) and silver (Sauer et al., 2002) have been reported.

Sol–gel provides an alternative synthesis route for nanomaterial fillings in porous alumina nanoholes. Monodisperse hollow nanocylinders containing crystalline titania particles have been filled by an aqueous solution of titanium tetrafluoride (Imai et al., 1999). Hollow nanotubes comprising In_2O_3 and Ga_2O_3 were synthesized by sol–gel chemistry (Cheng & Samulski, 2001) and sol–gel synthesis of an array of C-70 single crystal nanowires in a porous alumina template was investigated (Cao et al., 2001a,b).

CVD deposition on porous alumina

Chemical vapor deposition of materials in porous alumina nanoholes is a challenging topic for CVD researchers. Since porous alumina can contain extremely high aspect ratio holes, it is of great interest to discover how high aspect ratio of holes can be filled by CVD. Working in a supercritical fluid medium is one way of obtaining excellent deposition profiles. Palladium films were synthesized at controlled depths within porous alumina disks by hydrogen reduction of organopalladium compounds dissolved in supercritical CO_2 at 60°C (Fernandes et al., 2001). Guided by a simple mass transport model, Pd films ranging from 2 to 80 μm in thickness were deposited at prescribed depths between 80 and 600 μm.

Carbon nanotube (CNT) CVD in porous alumina has been intensively studied by several groups recently (Li et al., 1999a,b; Iwasaki et al., 1999; Sung et al., 1999; Sui et al., 2002; Hu et al., 2001; 2002; Wang et al., 2002). It is well known that CNT–CVD needs catalysis for thermal decomposition of precursors. Li et al. (1999a,b) used electrodeposited Co as a precursor, while Iwasaki et al. (1999) used Nb located beneath the aluminum layer as a precursor. A SEM micrograph of a well-ordered array of CNT is shown in

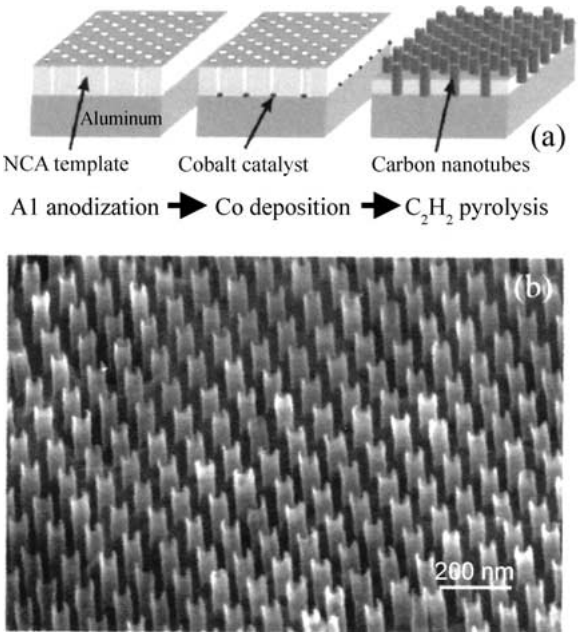

Figure 6. SEM image of array of carbon nanotube fabricated in porous alumina template (Li et al., 1999).

Figure 6. Using Co catalysis, pyrolysis of C_2H_2 was carried out at 650°C. CNTs with diameters ranging from 10 to several hundred nanometers and lengths of up to 100 μm can be produced. This structure is highly promising for an ultrahigh-density field emitter array. CNT formed through Co catalysis by this method has a multi-walled structure (Hu et al., 2002). Wang X.H. et al. (2000) reported low-temperature deposition of CNTs at around 520°C by microwave plasma assisted CVD.

Functional optical nanomaterials embedded in porous alumina

There have been many attempts to fill semiconductor materials in porous alumina nanoholes in an effort to produce highly luminescent materials. Although they are still slightly too large to exhibit the quantum confinement effect, nanoholes have excellent luminescent properties not found in bulk materials. We ought to begin our discussion by considering the photoluminescence (PL) properties of the porous alumina nanohole array itself. Du et al. (1999) investigated PL properties of porous alumina membranes fabricated by anodic oxidation using oxalic acid or sulfuric acid. They found

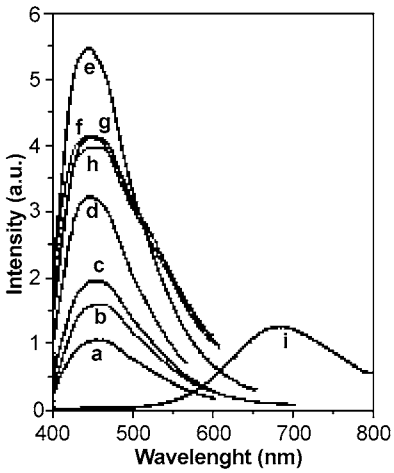

Figure 7. Photoluminescence spectra of a porous alumina membrane prepared in oxalic acid. (a) as prepared, (b) 200°C × 4 h, (c) 300°C × 4 h, (d) 400°C × 4 h, (e) 500°C × 4 h, (f) 550°C × 4 h, (i) porous Si (Du et al., 1999).

a blue PL band in the wavelength range of 400–600 nm, with an intensity peak at 460 nm. This band originates from singly ionized oxygen vacancies (F^+ center) in porous alumina membranes. The PL intensity of a porous alumina film was increased by annealing at a higher temperature as shown in Figure 7. It can be seen that the PL intensity of the porous alumina film fabricated using oxalic acid and annealed above 400°C is stronger than that of porous silicon. The PL intensity of porous alumina fabricated using oxalic acid was much stronger than that fabricated using sulfuric acid.

Enhanced PL was observed by filling titania doped with Terbium (Tb) or Erbium (Eb) (Gaponenko et al., 2000; 2001). An assembly of ZnO nanoparticles was synthesized by immersing the porous alumina membrane in a mixture of zinc butanol and water at 60°C and then heating at 200°C (Shi et al., 2000). PL measurements showed a peak at 485 nm. Compared with the PL spectra of nanostructured bulk ZnO, the PL intensity of ZnO nanoparticles in the alumina membrane is enhanced by a factor of 20 (Figure 8). This arises from the increase in singly ionized oxygen vacancies (F-centers) in the ZnO nanoparticles located within the pores of the alumina membrane. A CdS nanowire array fabricated by electrodeposition exhibited three ultraviolet PL bands and one yellow–green PL band (Wang et al., 2002). GaN nanoparticles filled by sol–gel synthesis showed excellent PL properties (Chen et al., 2001; Cheng et al.,

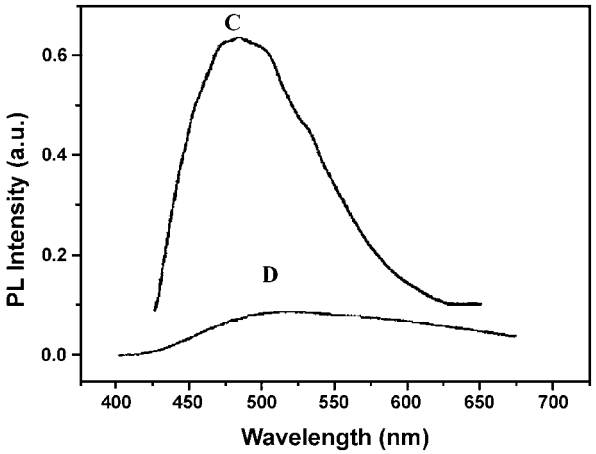

Figure 8. The PL spectra induced by the nano-ZnO particles in the assembly (curve C), and of he nanostructured ZnO bulk (curve D) (Shi et al., 2000).

1999). A laser dye, rhodamine 6G (RG6), and another luminescent organic molecule, 8-hydroxyquinoline aluminum (Alq(3)), were impregnated into porous alumina nanoholes (Xu et al., 2002). A clearly blue-shifted PL was observed for both the Alq(3) and RG6 contained within the nanoholes. The measured spectral characteristics demonstrate the influence of pore size on the emission of the organic molecules. These studies suggest that porous alumina films have a high potential for use in electroluminescent devices. Kukhta et al. (2002) proposed a simple method for attaching electrodes to nanomaterials embedded in nanoholes. The bottom part of the alumina layer, placed between the aluminum and pore space, is removed by a slow reduction in anodic voltage down to zero. The schema of the structure, and an SEM micrograph of the nanohole bottom after bottom opening are shown in Figure 9. The use of a porous alumina cathode results in a less homogeneous electric field, and hence, more intensive auto-electron emission and higher cathode efficiency. Luminescent organic molecules were adsorbed on the walls of the cylindrical pores, causing a significant increase in luminophor concentration. These organic electroluminescent devices can easily be manufactured and they are more efficient and stable as compared with the usual layered structures.

Photonic band crystals have been intensively studied in order to develop nonlinear optical wave-guides. Porous alumina membrane is one of most promising two-dimensional (2-D) photonic crystal materials. The pretexturing technique has been employed to fabricate

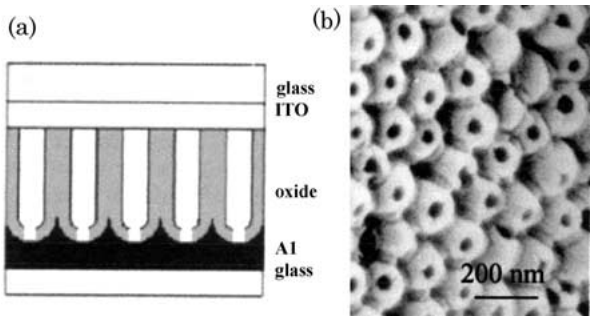

Figure 9. (a) A model of the organic electroluminescent cell, (b) SEM micrograph of the porous alumina bottom after opening the bottom barrier layer (Kukhta et al., 2002).

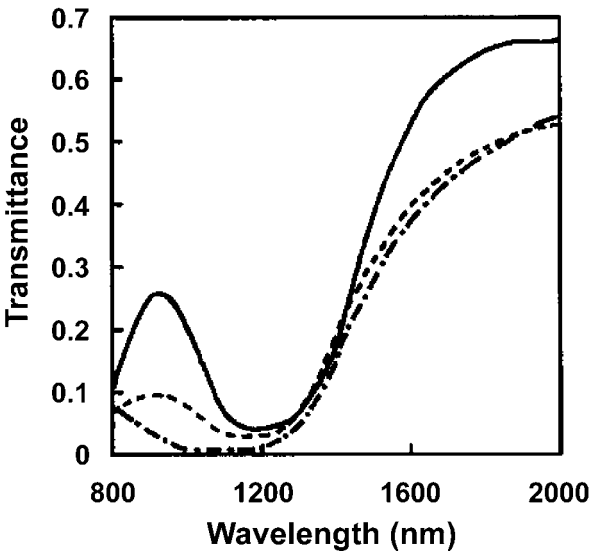

Figure 10. Transmission spectra of naturally ordered porous alumina for H-polarization light. The average interval of the air holes was 500 nm (Masuda et al., 2001).

large, single-domain alumina nanohole arrays to be used as 2-D photonic band crystals. A common optical grating is used to prepattern the aluminum substrate, which is subsequently anodized under mild conditions to yield an AOF with a photonic band gap in the visible region (Wehrspohn & Schilling, 2001; Mikulskas et al., 2001). The 2-D photonic crystals were fabricated using self-organized porous alumina with a high aspect ratio of over 200. The transmission properties of the resultant ordered air-hole array in the alumina matrix exhibited a stop band in the spectrum that corresponded to the band gap in 2-D photonic crystals as shown in Figure 10 (Masuda et al., 1999; 2000).

Magnetic nanomaterials embedded in porous alumina

Magnetic materials embedded in porous alumina matrix have a long history (Kawai & Ishiguro, 1975). The main purpose of these studies is to realize a high-density magnetic recording media. Soon, the recording density of a magnetic hard disk will exceed 100 Gbit/in^2, and materials for 1 terabit/in^2 are strongly required. A dense array of magnetic nanoparticles is considered to be the most promising candidate (Sun et al., 2001), however, it is difficult to obtain perpendicular magnetic anisotropy by nanoparticles. Magnetic nano-rods or -dots embedded in porous alumina nanoholes satisfy the requirement for perpendicular anisotropy because magnetic rods with a high aspect ratio (ratio of height to diameter) can easily be formed in a porous alumina template. Ni (Nielsch et al., 2000; 2002b; Zheng et al., 2000; 2002; Metzger et al., 2001; Kroll et al., 2001), Co (Metzger et al., 2001; Sun et al., 2000; 2001; Kroll et al., 2001; Strijkers et al., 1999), Fe (Metzger et al., 2001; Kroll et al., 2001; Menon et al., 2000), and alloys such as CoFe (Menon et al., 2001), NiCo (Zhu et al., 2001) were filled into porous alumina by pulsed or AC electrodeposition and their magnetic properties were determined. In most cases, magnetic nanorods with diameters ranging from 10 to 60 nm, and nearest neighbor distances between 60 and 120 nm were fabricated by porous alumina prepared by oxalic acid or sulfuric acid anodic oxidation. A typical cross-sectional TEM image of a nanomagnet array is shown in Figure 11, where polycrystalline Co dots with a diameter of 40 nm were formed (Metzger et al., 2001). Using a porous alumina template, we can control the height of ferromagnetic dots by deposition time. Figure 12 shows M-H hysteresis loops of a Co particle array with a height of (a) 5 nm, and (b) 60 nm. There is a clear difference in the magnetic anisotropy; the thinner Co rods (length = 5 nm) have a rather in-plane anisotropy, while the thicker rods (length = 220 nm) have an out-of-plane anisotropy. Thus, the magnetic anisotropy of ferromagnetic rods is mainly governed by shape. The structure of the Co rods was investigated with nuclear magnetic resonance, which revealed that the wires exhibit a mixture of fcc and hcp texture with the (0001) texture of the hcp fraction oriented preferentially perpendicular to the wires (Nielsch et al., 2000). These features are common to all ferromagnetic metals. In the case of Fe rods, the existence of a critical diameter for which the coercivity has a maximum was observed at room temperature (Menon et al., 2000). The maximum coercivity obtained at room temperature is 2640 Oe. However, there was no maximum in coercivity as a function of diameter at 5 K. Controllability of alloy composition by electroplating is good to the $Fe_{1-x}Co_x$ ($0 < x < 1$) alloy system studied by Menon et al. (2001). The crystal structure is bcc at the Fe end. As the Co content increases, the crystal structure remains bcc until about 67% Co, above which the structure transforms into a mixture of hcp and fcc. For $Fe_{0.67}Co_{0.33}$ nanorods with a diameter of 9 nm, the coercivity is about 2900 Oe, whereas for $Fe_{0.33}$–$Co_{0.67}$ nanowires, it is about 2850 Oe. Temperature and size dependence of magnetic properties show no indication of superparamagnetic effects down to a wire diameter of 9 nm. For a nanomagnet array density of above 1 terabit/in^2, a nanohole pitch below 25 nm is required. This is currently not achievable through self-organization of porous alumina nanohole arrays, and would require further technological breakthrough.

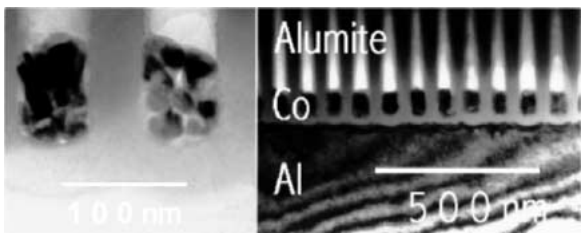

Figure 11. TEM cross-section of porous alumina and Co particles at the bottom of pores (Sun M. et al., 2001).

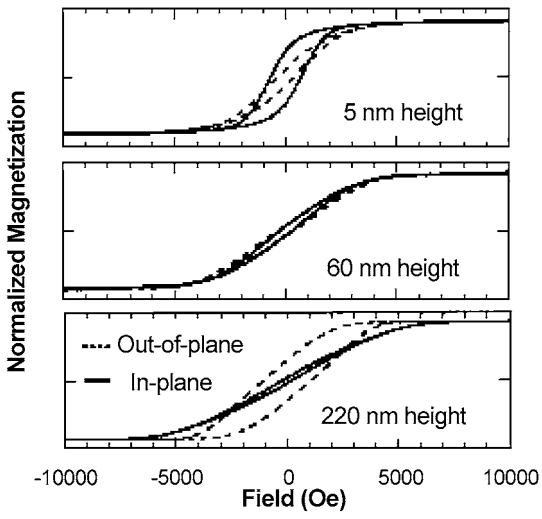

Figure 12. M–H hysteresis loops of Co particle array: (a) 5 nm long, (b) 60 nm long (Sun M. et al., 2001).

Nanostructure formation on solid substrate: Toward electron devices

Several authors have discussed fabrication of nanoscaled electron devices using porous alumina templates. A relatively easy application is a field emitter array (Govyadinoc & Zakhvitcevich, 1999; Hu et al., 2001), as the technique enables the fabrication of ultrahigh-density emitter arrays. Carbon nanotube arrays (Hu et al., 2002) and other metal arrays (Govyadinoc & Zakhvitcevich, 1999) were proposed. A comprehensive overview of electronic device applications was reported by Routkevitch et al. (1996). Fabrication of one-dimensional metal or semiconductor (CdS, CdS_xSe_{1-x}, $Cd_xZn_{1-x}S$, GaAs) wires and one-dimensional superlattices was proposed. Electron tunneling phenomena via the nanohole bottom barrier layer was observed for the first time (Routkevitch et al., 1996), which showed a stepwise increase in conductance with increasing voltage in the Al/alumina bottom barrier film/Ni wire/NiO/Ag system. The Coulomb blockade phenomenon with a single tunneling barrier was observed in a similar structure at low temperature (Haruyama & Sato, 2000; Haruyama et al., 2000).

Transport property of CNT grown in porous alumina nanoholes has been investigated by several authors. Li et al. (1999b) grew sophisticated Y-junction CNT arrays. The Y-junction CNTs were produced by CVD growth catalyzed by electrodeposited Co in branched porous alumina template. The branch was made by a sudden decrease in the anodic voltage, which was very efficient in the anodic oxidation for the change in nanohole diameter as well as pitch. Transport measurements showed an reproducible rectifying behavior at room temperature (Papadopoulos et al., 2000). The result was well explained by a junction with an abrupt change in band gap due to the nanotube diameter, and possibility for a new heterojunction devices were suggested. Haruyama et al. (2001a,b,c; 2002) further investigated low temperature conductance properties of CNTs buried in porous alumina nanoholes. Coulomb blockade related localization effect in a single tunnel-junction/CNT system, and anomalous localization effects associated with excess Co catalyst diffused in multiwalled carbon nanotubes (MWNTs) were observed. Further they slightly diffuse atoms of electrode materials into one end of MWNTs, grown using nanoporous alumina membranes. Diffusion of the light-mass materials lead to weak localization in Altshuler–Aronov–Spivak oscillation. In contrast, diffusion of heavy-mass materials at the volume ratio of only about 5% change this weak localization to antilocalization, and they proposed an electron-wave phase switching circuit using this effect.

Kouknin et al. (2000) observed an unexpected electronic bistability in the current–voltage characteristics of CdS-embedded porous alumina with current paths in both the lateral and vertical directions. However, the mechanism behind this bistable switching phenomenon remains unclear. They also observed an extremely high photoresistivity in CdS and ZnSe nanowires electrodeposited onto a porous alumina film. The resistance of these nanowires increases by one to two orders of magnitude when exposed to infrared radiation, possibly because of real-space transfer of electrons from the nanowires into the surrounding alumina by photon absorption (Kouklin et al., 2001).

The above-mentioned studies of electronic devices utilize porous alumina fabricated on alumina plates. Thus, it is difficult to apply them to devices in integrated circuits. Shingubara was the first to study porous alumina nanohole array formation on Si substrates (Shingubara et al., 1999). They sputtered a thick (20 μm) pure aluminum film on a SiO_2/Si substrate, and carried out the two-step anodic oxidation of aluminum. By keeping the aluminum surface flat during sputtering, a well-ordered array of nanoholes was fabricated. In this method, the electrode makes contact with the aluminum film during anodic oxidation. If the SiO_2 layer is thin enough to allow tunneling current and a heavily doped Si substrate with low resistivity is used, electrode can be made using the backside of a Si wafer. In later years, porous alumina films were formed on conductive solid substrates, such as ITO (indium tin oxide) (Chu et al., 2002) and n-type Si without SiO_2 layer (Crouse et al., 2000). SEM images of nanohole bottom on ITO and Si are shown in Figure 13. The nanohole bottom differs from those formed on aluminum; a void is formed underneath the bottom barrier layer of alumina in both cases. The SEM image of the bottom barrier layer formed on SiO_2 is shown in Figure 14 (Shingubara et al., 2002a,b). In contrast to Figure 13, the interface between the porous alumina barrier layer and the SiO_2 layer is flat, and aluminum islands remain at the interface. By further anodic oxidation, these aluminum islands are completely oxidized and diminished since anodically formed alumina film is an ionic conductor. The porous alumina bottom morphology varies depending on whether the under-layer is conductive or not. The void formation underneath the bottom barrier is thought to be caused by dissolution of alumina at the interface due to the high ionic current

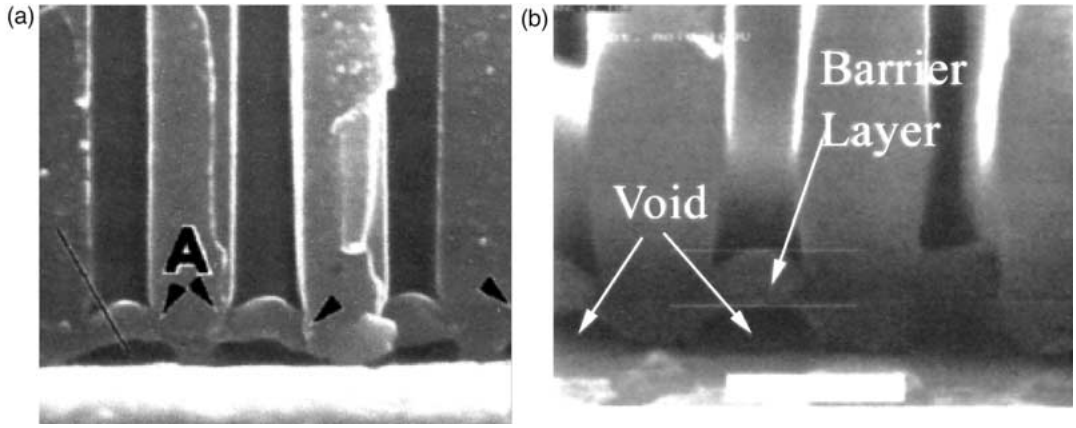

Figure 13. SEM micrographs of porous alumina nanohole bottom on (a) ITO (Chu et al., 2002), and (b) n-Si (Crouse et al., 2000).

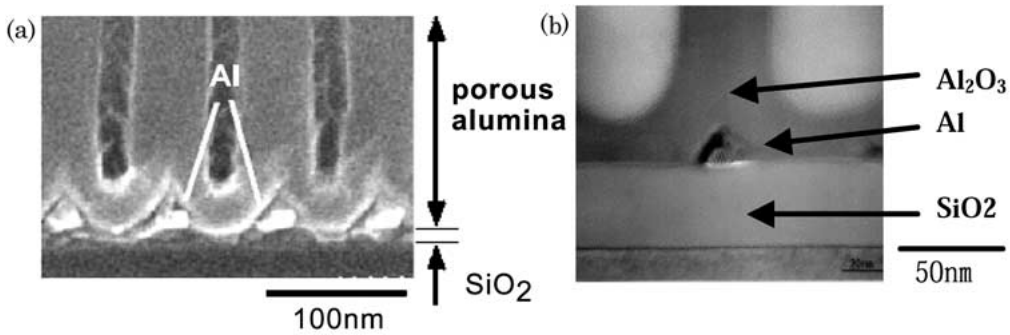

Figure 14. Cross-sectional observation of porous alumina nanohole bottom on SiO_2 formed by 0.15 M oxalic anodization of 40 V. (a) SEM micrograph, (b) TEM micrograph (Shingubara et al., 2002).

flowing perpendicular to the interface. An excellent hexagonal aluminum dot array was observed on SiO_2 upon completion of the anodic oxidation of the sputtered aluminum film as shown in Figure 15. The dot diameter and height are 40 and 15 nm, respectively. The space between dots is controlled by additional anodic oxidation time. Each dot can be used as a single electron memory node. Characteristics of the conduction between aluminum dots was recently measured; Coulomb blockade caused by single electron tunneling between aluminum dots was observed at liquid He temperatures (Shingubara et al., 2002c). Bandyopadhyay (2001) proposed qubit operations for quantum computers by the use of porous alumina. Universal 2-qubit operations are possible by a gate consisting of two trilayered quantum dots that are electrochemically synthesized within two adjacent pores in a porous alumina film. The two outer layers are ferromagnetic metals or semiconductors while the middle layer is a semiconductor with long spin coherence time (e.g., silicon).

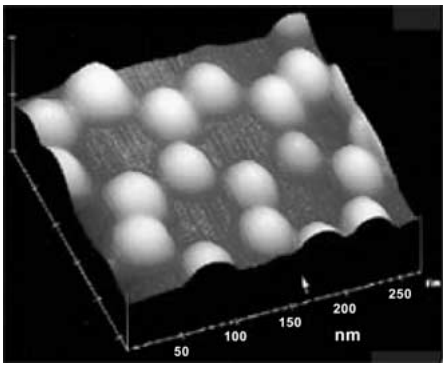

Figure 15. AFM image of aluminum hexagonal dot array formed at the interface between porous alumina and SiO_2 (Shingubara et al., 2002).

A single electron is injected into the middle semiconductor layer and its spin encodes a qubit.

In silicon ultra large scale integrated circuit (ULSI) technology, low dielectric constant materials are

urgently required. Porous alumina has high potential as a low dielectric constant material because its porosity can be controlled by a pore widening treatment using diluted phosphoric acid. The fundamental idea had been proposed by IBM in the early stages of integrated circuit (IC) development (Schwartz & Platter, 1975). However, this aspect was reconsidered recently for dielectric film applications (Lazarouk et al., 2000a,b). A low dielectric constant of about 2.4 was attained by chemical etching of porous alumina films in an anodizing solution. The intralevel insulator based on porous alumina was found to have the following properties: the breakdown voltage was above 400 V and the leakage current at an applied voltage of 15 V was below 10^{-9} A/cm^{-2}. A study on thermal overheating under high current density operation has shown that the developed structure offers advantages over aluminum interconnection passivated by silica insulator. The developed processing technique was tested for CMOS submicron technology. The fabricated aluminum-porous alumina structure demonstrated good chemical and thermal stability, and excellent adhesion to the layers above and below it.

Membranes and chemical sensors

Porous alumina films can be used as membranes with nanopore channels of extremely narrow size distribution. Shawaqfeh and Baltus (1999) formed a membrane by post-oxidation processing that removed unoxidized aluminum as well as the barrier layer of alumina. They made bilayer composite membranes by varying the current density during the oxidation process. The hydraulic permeability of membranes formed in phosphoric acid and the diffusive permeability of membranes formed in sulfuric acid were measured. These measured values showed excellent agreement with predicted values determined by kinetic studies.

Another method for the preparation of nanoporous membranes from anodically oxidized aluminum was described by Mozalev et al. (2001). Pores of an existing free anodic alumina film were protected with gelatin gel, and the oxide barrier layer was chemically dissolved from the bottom of the film. The membranes thus produced were examined as electrolyte carriers/separators for Li rechargeable batteries by impedance and cyclic charge/discharge measurements. Repeated electrodeposition–dissolution of Li on Ni and Al substrates in a LiPF6/propylene carbonate electrolyte was performed through the alumina membrane. Furthermore, transport behavior of monovalent and divalent solutes across mesoporous nanopore alumina membranes was investigated as a function of pore diameter, pH and ionic strength (Bluhm et al., 1999). Trace amounts of the radiotracers Cs-137, Sr-85, Na-22 and Ca-45 were present in the feed solutions at

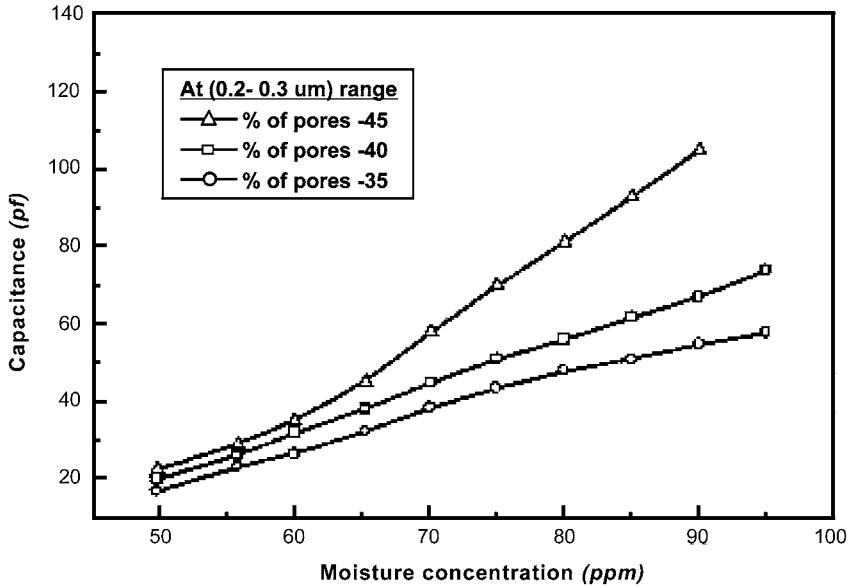

Figure 16. Capacitance response of moisture sensors made by porous alumina with various porosity (Basu et al., 2001).

concentrations ranging from 10^{-9} to 10^{-12} M with total salt concentrations from 0.1 to 10^{-4} M. The divalent cations Ca^{2+} and Sr^{2+} exhibited lower diffusion rates than the monovalent cations Cs^{+} and Na^{+} for membranes with 20 nm diameter pores. This difference was attributed to the Donnan exclusion effect due to the positively charged alumina surface.

It is well known that the electrical properties of porous alumina are sensitive to moisture. Thus, it can potentially be used as a humidity sensor. Basu et al. (2001) proposed a new type of micro-humidity sensor based on porous alumina. They developed a moisture sensor based on porous alumina with interdigitated metallic electrodes for the measurement of moisture concentration in the 50–100 ppm range. Figure 16 shows the capacitor response of the interdigitated sensors. There is an almost linear relationship between moisture concentration and capacitance. The sensors have good sensitivity and are highly reproducible.

Concluding remarks

Porous alumina template has a high potential for use in a diversity of applications, including electronic devices, magnetic storage disks, sensors, and biological membranes. However, there are some problems that need urgent attention: (1) the pitch of a highly ordered nanohole array formed by self-organization is still limited, (2) a method to control nanohole diameters below 5 nm for observing the quantum confinement effect has yet to be devised and (3) a fabrication procedure for integrating porous alumina nanohole membranes on semiconductor solid substrates, while at the same time maintaining their mechanical stability, has not yet been established. The full potential of porous alumina in nano-sciences and technologies can only be realized through persistent efforts at solving these problems.

References

Asada T., 1969. Japanese Patent. No. 824505.

Asoh H., K. Nishio, M. Nakao, A. Yokoo, T. Tamamura & H. Masuda, 2001. Fabrication of ideally ordered anodic porous alumina with 63 nm hole periodicity using sulfuric acid. J. Vac. Sci. Technol. B19, 569.

Bandyopadhyay S., 2001. A nanospintronic universal quantum gate. Physica E 11, 126.

Basu S., S. Chatterjee, M. Saha, S. Bandyopadhyay, K.K. Mistry & K. Sengupta, 2001. Study of electrical characteristics of porous alumina sensors for detection of low moisture in gases. Sensors and Actuators, B-Chemical 79, 182.

Bluhm E.A., E. Bauer, R.M. Chamberlin, K.D. Abney, J.S. Young & G.D. Jarvinen, 1999. Surface effects on cation transport across porous alumina membranes. Langmuir 15, 8668.

Cao H.Q., Y. Xu, J.M. Hong, H.B. Liu, G. Yin, B.L. Li, C.Y. Tie & Z. Xu, 2001a. Sol–gel template synthesis of an array of single crystal CdS nanowires on a porous alumina template. Adv. Mater. 13, 1393.

Cao H.Q., Z. Xu, X.W. Wei, X. Ma & Z.L. Xue, 2001b. Sol–gel synthesis of an array of C-70 single crystal nanowires in a porous alumina template. Chem. Commun. 6, 541.

Chen L., A.J. Yin, J.S. Im, A.V. Nurmikko, J.M. Xu & J. Han, 2001. Fabrication of 50–100 nm patterned InGaN blue light emitting heterostructures. Physica Status Solidi A 188, 135.

Cheng G.S., L.D. Zhang, X.G. Zhu, S.H. Chen, Y. Li, Y. Zhu & G.T. Fei, 1999. Synthesis of orderly nanostructure of crystalline GaN nanoparticles on anodic porous alumina membrane. Nanostruct. Mater. 11, 421.

Cheng B. & E.T. Samulski, 2001. Fabrication and characterization of nanotubular semiconductor oxides In_2O_3 and Ga_2O_3. J. Mater. Chem. 11, 2901.

Chu S.Z., K. Wada, S. Inoue & S. Todoroki, 2002. Formation and microstructures of anodic alumina films from aluminum sputtered on glass substrate. J. Electrochem. Soc. 149, B321.

Crouse D., Y.-H. Lo, A.E. Miller & M. Crouse, 2000. Self-ordered pore structure of anodized alumina on silicon and pattern transfer. Appl. Phys. Lett. 76, 49.

Du Y., W.L. Cai, C.M. Mo, J. Chen, L.D. Zhang & X.G. Zhu, 1999. Preparation and photoluminescence of alumina membranes with ordered pore arrays. Appl. Phys. Lett. 74, 2951.

Fernandes N.E., S.M. Fisher, J.C. Poshusta, D.G. Vlachos, M. Tsapatsis & J. J. Watkins, 2001. Reactive deposition of metal thin films within porous supports from supercritical fluids. Chem. Mater. 13, 2023.

Gaponenko N.V., J.A. Davidson, B. Hamilton, P. Skeldon, G.E. Thompson, X. Zhou & J.C. Pivin, 2000. Strongly enhanced Tb luminescence from titania zerogel solids mesoscopically confined in porous anodic alumina. Appl. Phys. Lett. 76, 1006.

Gaponenko N.V., O.V. Sergeeve, E.A. Stepanova, V.M. Parkun, A.V. Mudryi, H. Gnaser, J. Misiew, L.J. Balk & G.E. Thompson, 2001. Optical and structural characterization of erbium-doped TiO_2 xerogel films processe on porous anodic alumina. J. Electrochem. Soc. 148, H13.

Govyadinoc A.N. & S.A. Zakhvitcevich, 1999. Field emitter arrays based on natural self-organized porous anodic alumina. J. Vac. Sci. Technol. B16, 1222.

Gphausen H.J. & G.C. Schoener, 1984. Plating and Surf. Finishing 71, 56.

Haruyama J. & Y. Sato, 2000, Influence of phase fluctuation in external environment on coulomb blockade an array system of single tunnel junctions/Ni nanowires. Appl. Phys. Lett. 76, 1698.

Haruyama J., K. Hijioka, M. Tako & Y. Sato, 2000. Coulomb blockade related to mutual coulomb interaction in an external environment in an array of single tunnel junctions connected to Ni nanowires. Phys. Rev. B. 62, 8420.

Haruyama J., I. Takesue, S. Kato, K. Takazawa & Y. Sato, 2001a. Mesoscopic phenomena in nano-porous alumina films: single

nano-tunnel junctions connected to Ni-nanowires and carbon nanotubes. Appl. Surf. Sci. 175–176, 597.

Haruyama J., I. Takesue, T. Hasegawa & Y. Sato, 2001b. Coulomb blockade related to a localization effect in a single tunnel-junction/carbon-nanotube system. Phys. Rev. B 63, 073406.

Haruyama J., I. Takesue & T. Hasegawa, 2001c. Drastic change of phase interference by small diffusion of heavy-mass electrode atoms in carbon nanotubes and phase switching device. Appl. Phys. Lett. 79, 269.

Haruyama J., I. Takesue & T. Hasegawa, 2002. Anomalous localization effects associated with excess volume of cobalt catalyst in multiwalled nanotubes. Appl. Phys. Lett. 81, 3031.

Hoar T.P. & N.F. Mott, 1959. A mechanism for the formation of porous anodic oxide films on aluminium. J. Phys. Chem Solids 9, 97.

Hu W.C., L.M. Yuan, Z. Chen, D.W. Gong & K. Saito, 2002. Fabrication and characterization of vertically aligned carbon nanotubes on silicon substrates using porous alumina nanotemplate. J. Nanosci. Nanotechnol. 2, 203.

Hu W., D. Gong, Z. Chen, C.A. Grimes & P. Kichambare, 2001. Growth of well-aligned carbon naotube arrays on silicon substrates using porous alumina film as a nanotemplate. Appl. Phys. Lett. 79, 3083.

Imai H., Y. Takei, K. Shimizu, M. Matsuda & H. Hirashima, 1999. Direct preparation of anatase TiO_2 nanotube in porous alumina membranes. J. Mater. Chem. 9, 2971.

Iwasaki T., Y. Motoi & T. Den, 1999. Multiwalled carbon nanotubes growth in anodic alumina nanoholes. Appl. Phys. Lett. 75, 2044.

Jessensky O., F. Muller & U. Gosele, 1998a. Self-organized formation of hexagonal pore arrays in anodic alumina. Appl. Phys. Lett. 72, 1173.

Jessensky O., F. Muller & U. Gosele, 1998b. Self-organized formation of hexagonal pore structures in anodic alumina. J. Electrochem. Soc. 145, 3735.

Kawai S. & I. Ishiguro, 1975. Magnetic properties of anodic oxide coatings on aluminum containing electrodeposited Co and Co–Ni. J. Electrochem. Soc. 122, 32.

Kawai S. & I. Ishiguro, 1976. Recording characteristics of anodic oxide films on aluminum containing electrodeposited ferromagnetic metals and alloys. J. Electrochem. Soc. 123, 1047.

Keller F., M.S. Hunter & D.L. Robinson, 1953. Structural features of oxide coatings on aluminum. J. Electrochem. Soc. 100, 411.

Kouklin N., S. Bandyopadhyay, S. Teresin, A. Varfolomeev & D. Zaretsky, 2000. Electronic bistability in electrochemically self-assembled quantum dots: A potential nonvolatile random access memory. Appl. Phys. Lett. 76, 460.

Kouklin N., L. Menon, A.Z. Wong, D.W. Thompson, J.A. Woollam, P.F. Williams & S. Bandyopadhyay, 2001. Giant photoresistivity and optically controlled switching in self-assembled nanowires. Appl. Phys. Lett. 79, 4423.

Kroll M., L.J. de Jongh, F. Luis, P. Paulus & G. Schmid, 2001. Magnetization reversal and magnetic anisotropy of Fe, Ni and Co nanowires in nanoporous alumina membranes. Mat. Res. Soc. Symp. Proc. 674., U4.5.1.

Kukhta A.V., G.G. Gorokh, E.E. Kolesnik, A.I. Mitkovets, M.I. Taoubi, Y.A. Koshin & A.M. Mozalev, 2002. Nanostructured alumina as a cathode of organic light-emitting devices. Surf. Sci. 507, 593.

Lazarouk S., S. Katsouba, A. Demianovich, V. Stanovski, S. Voitech, V. Vysotski & V. Ponomar, 2000a. Reliability of built in aluminum interconnection with low-epsilon dielectric based on porous anodic alumina. Solid State Electron. 44, 815.

Lazarouk S., S. Katsouba, A. Leshok, A. Demianovich, V. Stanovski, S. Voitech, V. Vysotski & V. Ponomar, 2000b. Porous alumina as low-epsilon insulator for multilevel metallization. Microelectron. Eng. 50, 321.

Li J., C. Papadopoulos & J.M. Xu, 1999a. Highly-ordered carbon nanotube arrays for electronics applications. Appl. Phys. Lett. 75, 367.

Li J., C. Papadopoulos & J. Xu, 1999b. Growing Y-junction Carbon Nanotubes. Nature 402, 253.

Liang J., H. Chik, A. Yun & J. Xu, 2002. Two-dimensional lateral superlattices on anostructures: Nonlithographic formation by anodic membrane template. J. Appl. Phys. 91, 2544.

Masuda H. & K. Fukuda, 1995. Ordered metal nanohole arrays made by a two-step replication of honeycomb structures of anodic alumina. Science 268, 1466.

Masuda H., F. Hasegawa & S. Ono, 1997. Self-ordering of cell arrangement of anodic porous alumina formed in sulfuric acid solution. J. Electrochem. Soc. 144, L127.

Masuda H., H. Yamada, M. Saitoh, H. Asoh, M. Nakao & T. Tamamura, 1997. Highly ordered nanochannel-array architecture in anodic aloumina. Appl. Phys. Lett. 71, 2770.

Masuda H., K. Yada & A. Osaka, 1998. Self-ordering of cell configuration of anodic porous aloumina with large-size pores in phosphorous acid solution. Jpn. J. Appl. Phys. 37, L1340.

Masuda H., M. Ohya, H. Asoh, M. Nakao, M. Nohtomi & T. Tamamura, 1999. Photonic crystal using anodic porous alumina, Jpn. J. Appl. Phys. Part2-Lett. 38, L1403.

Masuda H., M. Ohya, H. Asoh & K. Nishio, 2001. Photonic band gap in naturally occurring ordered anodic porous alumina. Jpn. J. Appl. Phys. 40, L1217.

Menon L., M. Zheng, H. Zeng, S. Bandyopadhyay & D.J. Sellmyer, 2000. Size dependence of the magnetic properties of electrochemically self-assembled Fe quantum dots. J. Electron. Mater. 29, 510.

Menon L., S. Bandyopadhyay, Y. Liu, H. Zeng & D.J. Sellmyer, 2001. Magnetic and structural properties of electrochemically self-assembled Fe1-xCox nanowires. J. Nanosci. Nanotechnol. 1, 149.

Metzger R.M., M. Sun, G. Zangari & M. Shamsuzzoha, 2001. Magnetic nanoparticle array with ultra-uniform length electrodeposited in highly ordered alumina nanopores (‘alumite’). Mat. Res. Soc. Symp. Proc. 636, D.9.33.1.

Mikulskas I., S. Juodkazis, R. Tomasiunas & J. G. Dumas, 2001. Aluminum oxide photonic crystals grown by a new hybrid method. Adv. Mater. 13, 1574.

Mozalev A., S. Magaino & H. Imai, 2001. The formation of nanoporous membranes from anodically oxidized aluminium and their application to Li rechargeable batteries. Electrochim. Acta 46, 2825.

Nakao M., S. Oku, T. Tamamura, K. Yasui & H. Masuda, 1999. GaAs and InP nanohole arrays fabricated by reactive beam etching using highly ordered alumina membrane. Jpn. J. Appl. Phys. 38, 1052.

Nielsch K., F. Muller, A.P. Li & U. Gosele, 2000. Uniform nickel deposition into ordered alumina pores by pulsed electrodeposition. Adv. Mater. 12, 582.

Nielsch K., J. Choi, K. Schwirn, R.B. Wehrspohn & U. Gosele, 2002a. Self-ordering regimes of porous alumina: The 10% porosity rule. Nano Lett. 2, 677.

Nielsch K., R. Hertel, R.B. Wehrspohn, J. Barthel, J. Kirschner, U. Gosele, S.F. Fischer & H. Kronmuller, 2002b. Switching behavior of single nanowires inside dense nickel nanowire arrays. IEEE Trans. Magn. 38, 2571.

O'Sullivan J.P. & G.C. Wood, 1970. Nucleation and growth of porous anodic films on aluminum. Proc. R. Soc. A317, 511.

Papadopoulos C., A. Rakitin, J. Li, A.S. Vedeneev & J.M. Xu, 2000. Electronic transport in y-junction carbon nanotubes. Phys. Rev. Lett. 85, 3476.

Routkevitch D., A.A. Tager, J. Haruyama, D. Almawlawi, M. Moskovits & J.M. Xu, 1996. Nonlithographic nano-wire arrays: Fabrication, physics, and device application. IEEE Trans. Electron Devices 43, 1646.

Sauer G., G. Brehm, S. Schneider, K. Nielsch, R.B. Wehrspohn, J. Choi, H. Hofmeister & U. Gosele, 2002. Highly ordered monocrystalline silver nanowire arrays. J. Appl. Phys. 91, 3243.

Schwartz G.C. & V. Platter, 1975. An anodic process for forming planar interconnection metallization for multilevel LSI. J. Electrochem. Soc. 122, 1508.

Shawaqfeh A.T. & R.E. Baltus, 1999. Fabrication and characterization of single layer and multi-layer anodic alumina membrane. J. Membrane Sci. 157, 147.

Shi G., C.M. Mo, W.L. Cai & L.D. Zhang, 2000. Photoluminescence of ZnO nanoparticles in alumina membrane with ordered pore arrays. Solid State Comm. 115, 253.

Shingubara S., O. Okino., H. Sakaue & T. Takahagi, 1997. Ordered two-dimensional nanowire array formation using self-organized nanoholes of anodically oxidized aluminum. Jpn. J. Appl. Phys. 36, 7791.

Shingubara S., O. Okino, Y. Sayama, H. Sakaue & T. Takahagi, 1999. Two-dimensional nanowire array formation on Si substrate using self-organized nanoholes of anodically oxidized aluminum. Solid State Electron 43, 1143.

Shingubara S., O. Okino, Y. Murakami, H. Sakaue & T. Takahagi, 2001. Fabrication of nanohole array on Si using self-organized porous alumnina mask. J. Vac. Sci. Technol. B19, 1901.

Shingubara S., Y. Murakami, K. Morimoto, H. Sakaue & T. Takahagi, 2002a. Formation of Al nanodot array by the combination of nano-indentation and anodic oxidation. Mat. Res. Soc. Symp. Proc. 705, 133.

Shingubara S., Y. Murakami, H. Sakaue & T. Takahagi, 2002b. Formation of Al dot hexagonal array on Si using anodic oxidation and selective etching. Jpn. J. Appl. Phys. 41, L340.

Shingubara S., Y. Murakami, K. Morimoto, G.R. Wu & T. Takahagi, 2002c. Aluminum nanodot array formation by anodic oxidation and its conduction properties. Extended Abst. 2002 Solid State Devices Mater. p. 266.

Shingubara S., Y. Murakami, K. Morimoto & T. Takahagi, 2003. Formation of aluminum dot array by combination of nanoindentation and anodic oxidation of aluminium. Surface Science (in press).

Sui Y.C., B.Z. Cui, R. Guardian, D.R. Acosta, L. Martinez & R. Perez, 2002. Growth of carbon nanotubes and nanofibres in porous anodic alumina film. Carbon 40, 1011.

Strijkers G.J., J.H.J. Dalderop, M.A.A. Broeksteeg, H.J.M. Swagten, & W.J.M. de Jonge, 1999. Structure and magnetization of arrays of electrodeposited Co wires in anodic alumina. J. Appl. Phys. 86, 5141.

Sun S., D. Weller & C.B. Murray, 2001. In: Plumer M.L., Ek J.v. and Weller D. eds. The Physics of Ultra-High-Density Magnetic Recording, Springer, New York, pp. 249–276.

Sun M., G. Zangari & R.M. Metzger, 2000. Cobalt island arrays with in-plane anisotropy electrodeposited in highly ordered alumite. IEEE Trans. Magn. 36, 3005.

Sun M., G. Zangari, M. Shamsuzzoha & M. Metzger, 2001. Electrodeposition of highly uniform magneticnanoparticle arrays in ordered alumite. Appl. Phys. Lett. 78, 2964.

Sung S.L., S.H. Tsai, C.H. Tseng, F.K. Chiang, X.W. Liu & H.C. Shih, 1999. Well-aligned carbon nitride nanotubes synthesized in anodic alumina by electron cyclotron resonance chemical vapor deposition. Appl. Phys. Lett. 74, 197.

Thompson G.E., R.C. Furneaux, G.C. Wood, J.A. Richardson & J.S. Goode, 1978. Nucleation and growth of porous anodic films on aluminum. Nature 272, 433.

Wang Y.H., Y. Q. Xu, W.L. Cai & J.M. Mo, 2002. New method to prepare CdS nanowire arrays. Acta Physico-Chim. Sinica 18, 943.

Wang X.H., Z. Hu, Q. Wu & Y. Chen, 2002. Low-temperature catalytic growth of carbon nanotubes under microwave plasma assistance. Catalysis Today 72, 205.

Wehrspohn R.B. & J. Schilling, 2001. Electrochemically prepared pore arrays for photonic-crystal applications. MRS Bull. 26, 623.

Xu C.X., Q.H. Xue, Y. Zhong, Y.P. Cui, L. Ba, B. Zhao & N. Gu, 2002. Photoluminescent blue-shift of organic molecules in nanometre pores. Nanotechnology 13, 47.

Zeng H., S. Michalski, R.D. Kirby, D.J. Sellmyer, L. Menon & S. Bandyopadhyay, 2002. Effects of surface morphology on magnetic properties of Ni nanowire arrays in self-ordered porous alumina, J. Phys. Cond. Matter. 14, 715.

Zheng M., L. Menon, H. Zeng, Y. Liu, S. Bandyopadhyay, R.D. Kirby & D.J. Sellmyer, 2000. Magnetic properties of Ni nanowires in self-assembled arrays. Phys. Rev. B 62, 12282.

Zhu H., S.G. Yang, G. Ni, D.L. Yu & Y.W. Du, 2001. Fabrication and magnetic properties of $Co_{67}Ni_{33}$ alloy nanowire array. Scripta Mater. 44, 2291.